Available online at www.sciencedirect.com

ScienceDirect

Procedia Engineering 81 (2014) 2159 – 2164

Procedia Engineering

www.elsevier.com/locate/procedia

11th International Conference on Technology of Plasticity, ICTP 2014, 19-24 October 2014, Nagoya Congress Center, Nagoya, Japan

Nanoporous nickel fabricated by dealloying of rolled Ni-Mn sheet

Masataka Hakamada*, Mamoru Mabuchi

Department of Energy Science and Technology, Graduate School of Energy Science, Kyoto University, Yoshidahonmachi, Sakyo, Kyoto 606-8501, Japan

Abstract

Metallic nanoporous architecture can be spontaneously attained by dealloying of a binary alloy. Nanoporous nickel are fabricated by dealloying rolled Ni-Mn sheet. Unlike Ni-Al alloy, the initial Ni-Mn alloys had good cold workability because of their fcc crystal structures. After the electrolysis of the alloys in $(NH_4)_2SO_4$ aqueous solution, nanoporous architecture of Ni with pore sizes of 10–20 nm was confirmed. Also, a nanoporous/bulk bilayer-stacked Ni electrochemical actuator sheet was fabricated. The stacked bilayer sheet composed of bulk and nanoporous Ni reversibly deformed when a potential of ±1 V was applied in aqueous NaOH solution. The electrochemical actuation is considered to have a strong relationship with the electrical double layer, because cyclic voltammetric measurements suggested that the effect of oxygen adsorption on the surface was minor. The results suggest that nanoporous Ni can be used as an actuator, and it has potential in being applied for commercial use because of its low price and high availability.

Selection and peer-review under responsibility of the Department of Materials Science and Engineering, Nagoya University

Keywords: Nickel; Manganese; Rolling; Actuator; Porous materials

1. Introduction

Nanoporous nickel can be obtained by the alkali leaching of aluminum from Ni-Al Raney nickel (Raney (1927)) and has been widely used in catalytic applications (Freel et al. (1969) and Robertson et al. (1972)). However, the porous structure derived from Raney nickel is nonuniform (Robertson et al. (1972) and Smith et al. (2001))

* Corresponding author. Tel.: +81-75-753-5606; fax: +81-75-753-5428.
E-mail address: hakamada.masataka.3x@kyoto-u.ac.jp

Selection and peer-review under responsibility of the Department of Materials Science and Engineering, Nagoya University
doi:10.1016/j.proeng.2014.10.302

probably due to Ni-Al intermetallics. The brittle intermetallics also limit the application of nanoporous nickel to the powder form. If the starting alloy is ductile, the desired macroscopic shape of the resulting nanoporous nickel can be formed by plastic deformation of the starting alloy, thus widening the range of forms in which the catalyst can be applied.

Hayes et al. (2006) succeeded in fabricating homogeneous nanoporous copper by dealloying Cu-Mn alloy. The binary phase diagram of the Cu-Mn system (Okamoto,1998) shows that a single-phase solid solution of face-centered cubic (fcc) Cu-γMn can be obtained by homogenization at a suitable temperature and subsequent rapid quenching. Inspection of the Ni-Mn binary phase diagram (Gokcen, 1991) also reveals that a single-phase solid solution of fcc Ni-γMn can be produced in a similar manner. Nickel is a nobler element than manganese, which can be easily understood by comparing their standard electrode potentials (Pourbaix, 1966); therefore, manganese can be readily dissolved from the starting Ni-Mn alloys. Hence, these alloys are promising starting materials for the fabrication of nanoporous nickel with a homogeneous structure and a desired macroscopic shape. In this presentation, we show the fabrication of nanoporous nickel by dealloying of Ni-Mn alloys (Hakamada and Mabuchi, 2009a). Furthermore, electrochemical actuation of nanoporous nickel sheet, which is one of the curious properties of nanostructured metals with high surface area, is exhibited (Hakamada et al., 2012).

2. Experimental procedure

2.1. Fabrication

Nickel and manganese with >99.9 mass% purity were used as raw materials. They were melted together in an Ar-atmosphere arc furnace to form starting alloy ingots of $Ni_{0.3}Mn_{0.7}$. For comparison, a $Ni_{0.3}Al_{0.7}$ alloy ingot was also fabricated in the same manner. The ingots were homogenized at 1173 K (or 1073 K for $Ni_{0.3}Al_{0.7}$) for 24 hours under an Ar atmosphere and then rapidly quenched in water. The room-temperature rolling of the ingots was challenged. A three-electrode electrochemical cell controlled by a potentiostat was used for anodic polarization measurements and dealloying. The quasi-static electrochemical behaviors of the rolled Ni-Mn alloy were examined by obtaining anodic polarization curves in 1 mol/l $(NH_4)_2SO_4$ electrolyte with a scan rate of 1 mV s^{-1}. The apparent area exposed to the electrolyte was 12 mm^2. To fully dealloy the rolled sheets, a constant electrochemical potential of −0.65 V vs a saturated calomel electrode was applied in 1 mol/l $(NH_4)_2SO_4$ for 1.5×10^5 s.

After rinsing with pure water, the dealloyed samples were observed using a scanning electron microscope (SEM). X-ray diffraction (XRD) analyses were also performed on samples using a Cu X-ray source for phase identification. For observation with a transmission electron microscope (TEM), a 3-mm-diameter disc was cut from initial rolled alloys. One side of the disc was polished and the other side was dimpled to a central thickness of 60 μm. The alloy disc was then dealloyed at −0.65 V vs SCE for 3.6×10^3 s in 0.1 mol/l $(NH_4)_2SO_4$ electrolyte, followed by thinning by Ar-ion milling apparatus.

2.2. Electrochemical actuation

The fabrication of the actuator sheet composed of a bulk and nanoporous Ni stacked bilayer is illustrated in Fig. 1. Ni was initially electrodeposited onto the rolled $Ni_{0.3}Mn_{0.7}$ sheet (rolling was conducted at room temperature with reduction of approximately 10% to a thickness of 200 μm). The electrolyte for the Ni electrodeposition was composed of $NiSO_4 \cdot 6H_2O$ (150 g/l) and $NiCl_2 \cdot 6H_2O$ (15 g/l), and the pH was adjusted to 4.0 using H_3BO_3. The working electrode and counter electrode were the Ni-Mn film and bulk Ni sheet, respectively. A direct current density of 30 mA cm^{-2} was applied for 1 h at 333 K. The Ni-electrodeposited Ni-Mn sheet was then heated at 773 K for 7.2×10^3 s under Ar flow, to allow diffusion bonding. The (Ni-Mn)/Ni sheet was then dealloyed in 1 mol/l $(NH_4)_2SO_4$ at room temperature. The counter electrode, working electrode and reference electrode were platinum wire, (Ni-Mn)/Ni sheet and saturated calomel electrode, respectively. An electrochemical potential of −0.65 V vs saturated calomel electrode was applied on the working electrode for 1.1×10^5 until very little current was detected. Cyclic voltammetry was conducted using a potentiostat and a typical three-electrode electrochemical cell, with a Pt plate counter electrode, saturated calomel electrode reference electrode and sample working electrode in

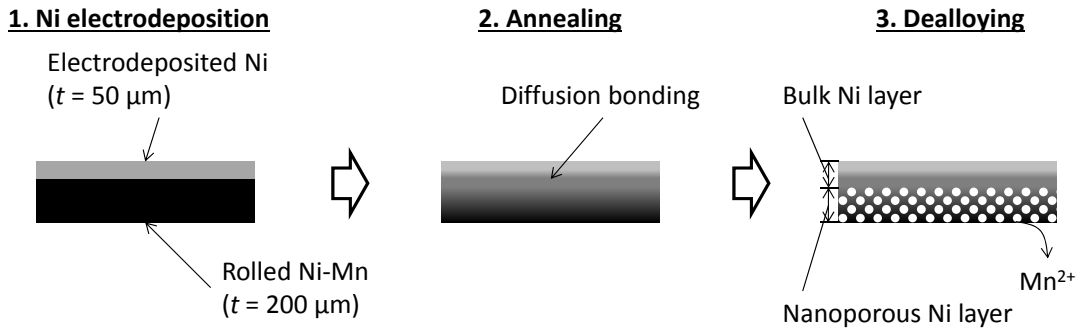

Fig. 1. Preparation of the nanoporous/bulk nickel stacked bilayer sheet. Permission from Elsevier (Hakamada et al. (2012)).

aqueous 1 mol/l NaOH solution. To determine the actuation in nanoporous Ni, the nanoporous/bulk Ni bilayer sheet (length, width and thickness of 40, 3 and 0.25 mm, respectively) (as a working electrode) was immersed in 1 mol/l NaOH. The counter electrode was Pt wire. The potential difference between the electrodes was switched from −1 to +1 V every 10 s, and the movement of the specimen was observed with a stereomicroscope. A strain gauge was pasted on the bulk Ni side of the specimen so that the strain was simultaneously monitored during switching of the applied potential (Loh and Chang, 2011).

3. Results and discussion

3.1. Fabrication

The ingot of $Ni_{0.3}Mn_{0.7}$ alloy was successfully cold-rolled to a thickness of approximately 0.2 mm, as exemplified in Fig. 2(a). However, when the $Ni_{0.3}Al_{0.7}$ ingot was subjected to cold rolling, it fractured without plastic deformation (Fig. 2(b)). The fcc single phases of Ni-Mn alloy is effective for enabling plastic deformation.

The anodic polarization curve for rolled Ni-Mn (not shown here because of space limitation) showed that the apparent current density almost monotonically increased with the applied potential. This trend is similar to the typical anodic polarization behaviors of Au-Ag (Sieradzki et al., 2002), Pt-Cu (Pugh et al., 2003) and Pd-Co (Hakamada and Mabuchi, 2009b) alloys in the electrolytes for fabrication of nanoporous metals. Thus, the common dealloying mechanism (Erlebacher, 2001) is operative in the $Ni_{0.3}Mn_{0.7}$ alloy in the electrolyte.

SEM and TEM images of the dealloyed $Ni_{0.3}Mn_{0.7}$ are given in Fig. 3. The dealloyed $Ni_{0.3}Mn_{0.7}$ sample had open-cell nanoporous structures with ligament and pore sizes of approximately 10 nm. TEM observations for nanoporous Ni gave more in-focus images than SEM observations. Electron diffraction patterns for the observed areas (shown in the insets of TEM images) suggest that the observed frames are essentially monocrystalline (Parida et al., 2006) in the region observed by TEM. Statistical analysis of 100 ligaments in the TEM images of nanoporous Ni reveals that the ligament size of nanoporous Ni was 8 nm ± standard deviation of 2 nm.

The XRD pattern for the nanoporous Ni is shown in Fig. 4. The XRD patterns of all dealloyed samples exhibited the peaks corresponding to fcc crystal structures. The peak intensity for the (220) planes were strongest in the patterns. The (220) orientation induced by the initial cold-rolling of $Ni_{0.3}Mn_{0.7}$ alloy is maintained during dealloying (Hakamada and Mabuchi, 2006).

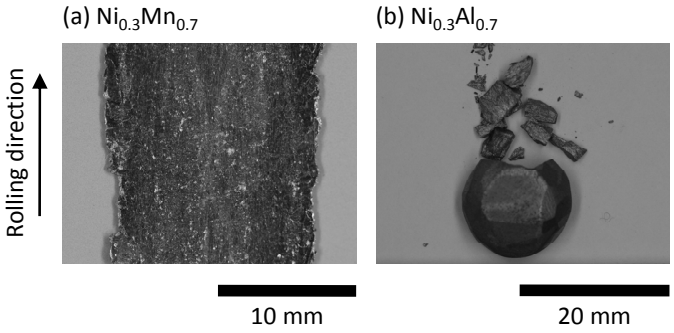

Fig. 2. (a) $Ni_{0.3}Mn_{0.7}$ and (b) $Ni_{0.3}Al_{0.7}$ alloys subjected to rolling at room temperature. Permission from Elsevier (Hakamada and Mabuchi (2009a)).

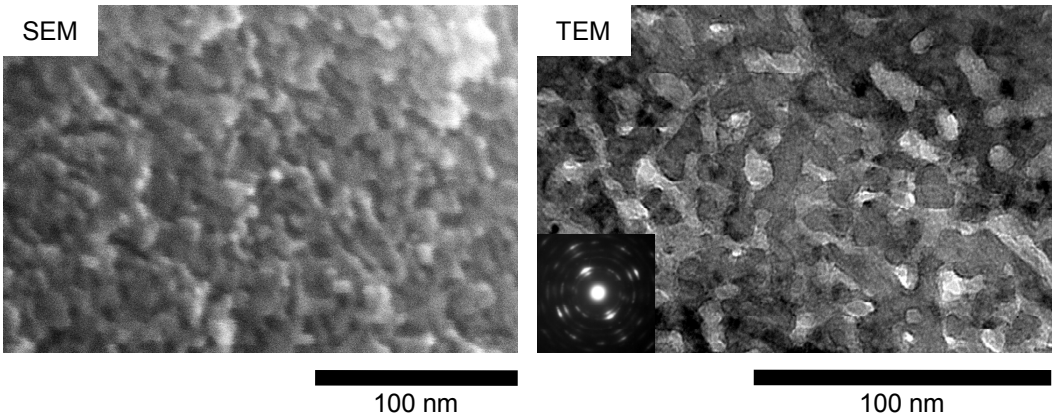

Fig. 3. Scanning (left) and transmission (right) electron micrographs of nanoporous nickel (dealloyed $Ni_{0.3}Mn_{0.7}$). Permission from Elsevier (Hakamada and Mabuchi (2009a)).

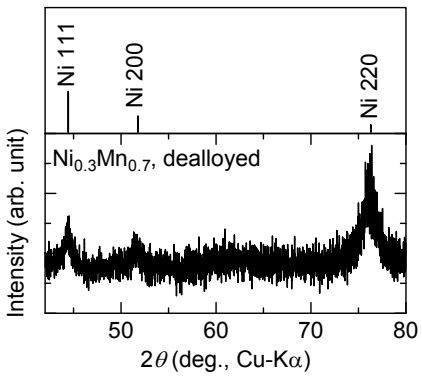

Fig. 4. XRD pattern of nanoporous nickel (dealloyed $Ni_{0.3}Mn_{0.7}$).

3.2. Electrochemical actuation

When the potential difference between the Pt electrode and nanoporous/bulk nickel electrode was switched from −1 to +1 V in the NaOH solution, the specimen moved reversibly in response to the changes in potential. The tip of the sheet moved by up to 0.5 mm.

The variation in strain during potential switching is shown in the left panel of Fig. 5, where the positive strain means the expansion of nanoporous layer. The strain was well-aligned with the voltage change; i.e. the strain increased when +1 V was applied and vice versa. A fast strain response was obtained, similar to the case reported for nanoporous Au (Kramer et al. (2004)).

The adsorption and desorption of oxygen have been reported to have an effect on the actuation (Jin et al., 2010) and mechanical response (Jin et al., 2011) of nanoporous gold. Cyclic voltammetry curves shown in the right panel of Fig. 5 show no clear peaks for the adsorption and desorption of oxygen, suggesting that oxygen sorption has a minor effect on the actuation of nanoporous nickel, although direct comparison between actuation (left panel in Fig. 5) and cyclic voltammetry (right panel in Fig. 5) is difficult because of the difference in the electrode setup (2-electrode and 3-electrode).

The dependence of surface stress on the surface charge density for a clean metal surface has been known as electrocapillarity (Kramer and Weissmüller, 2007), and theoretically predicted based on the jellium model (Haiss et al.,1998; Schmickler and Leiva, 1998). Therefore, nanoporous metals exhibit actuator characteristics because they have a large surface-to-volume ratio and considerable charge induced on their surface (Weissmüller et al., 2003; Kramer and Weissmüller, 2007). It has been clarified that modified bonding in the space-charge layer within the metal surface has an important effect on the change in surface stress (Weissmüller et al., 2003; Kramer et al., 2004; Schmickler and Leiva, 1998; Weigend et al., 2006). That is, induced charge varies the net charge in space-charge layers at the metal surface. Thus, the change in the electronic density of states leads to a change in surface stress. If this concept is valid, then each metallic species should exhibit different actuation behavior.

The coexistence of lattice expansion and contraction at the surface of nanoporous metals (Hakamada et al., 2010) may vary the electronic density of states of the surface. Therefore, we also consider that nanoporous metals exhibit actuator characteristics not only because they have a large surface area, but also because the electric density of states is changed by the disordered lattice at the surface (Weigend et al., 2006).

In the case of nanoporous gold and platinum, clean metallic surface state shows expansion under the positive potential sweeping (Jin et al., 2010), which was also observed in the present nanoporous nickel. On the other hand, according to Pourbaix diagram of nickel species (Pourbaix, 1966), contribution of hydrogen adsorption/desorption due to possible naturally-oxidized surface state of nickel should be taken into consideration.

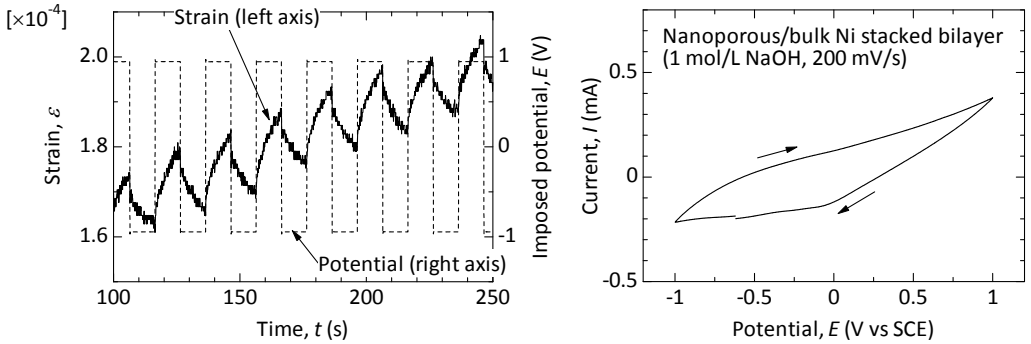

Fig. 5. (Left) Strain variation during potential switching of the nanoporous/bulk nickel actuator in aqueous NaOH. (Right) Cyclic voltammetry curve for the nanoporous/bulk nickel stacked bilayer in 1 mol/L NaOH. Permission from Elsevier (Hakamada et al., 2012).

4. Conclusions

Nanoporous nickel with pore size of ~10 nm can be fabricated by dealloying of ductile Ni-Mn rolled sheet. The cold-workability of initial alloy makes the application of nanoporous nickel wider. As one of the potential applications, the electrochemical actuation of nanoporous nickel in NaOH aqueous solution has been demonstrated, in which the strain varied sensitively with the change of induced potential.

References

Erlebacher, J., Aziz, M. J., Karma, A., Dimitrov, N., Sieradzki, K., 2001. Evolution of nanoporosity in dealloying. Nature 410, 450–453.

Freel, J., Pieters, W. J. M., Anderson, R. B., 1969. The structure of Raney nickel I. Pore structure. Journal of Catalysis, 14, 247–256.

Gokcen, N. A., 1991. The Mn-Ni (manganese-nickel) system. Journal of Phase Equilibria, 12, 313–321.

Haiss, W., Nichols, R. J., Sass, J. K., Charle, K. P., 1998. Linear correlation between surface stress and surface charge in anion adsorption on Au (111). Journal of Electroanalytical Chemistry 452, 199–202.

Hakamada, M., Mabuchi, M., 2009b. Fabrication of nanoporous palladium by dealloying and its thermal coarsening. Journal of Alloys and Compounds 479(1–2), 326–329.

Hakamada, M., Mabuchi, M., 2006. Nanoporous gold prism microassembly through a self-organizing route. Nano Letters 6, 882–885.

Hakamada, M., Mabuchi, M., 2009a. Preparation of nanoporous Ni and Ni-Cu by dealloying of rolled Ni-Mn and Ni-Cu-Mn alloys. Journal of Alloys and Compounds 485(1–2), 583–587.

Hakamada, M., Matsumura, S., Mabuchi, M., 2012. Electrochemical actuation of nanoporous Ni in NaOH solution. Materials Letters 70, 132–134.

Hakamada, M., Nakano, H., Furukawa, T., Takahashi, M., Mabuchi, M., 2010. Hydrogen storage properties of nanoporous palladium fabricated by dealloying. The Journal of Physical Chemistry C 114, 868–873.

Hayes, J. R., Hodge, A. M., Biener, J., Hamza, A. V., Sieradzki, K., 2006. Monolithic nanoporous copper by dealloying Mn-Cu. Journal of Materials Research, 21, 2611–2616.

Jin, H. J., Wang, X. L., Parida, S., Wang, K., Seo, M., Weissmüller, J., 2010. Nanoporous Au−Pt alloys as large strain electrochemical actuators. Nano Lett 10, 187–194.

Jin, H. J., Weissmüller, J., 2011. A material with electrically tunable strength and flow stress. Science 332, 1179–1182.

Kramer, D., Viswanath, R. N., Weissmüller, J., 2004. Surface-stress induced macroscopic bending of nanoporous gold cantilevers. Nano Letters 4, 793–796.

Kramer, D., Weissmüller, J., 2007. A note on surface stress and surface tension and their interrelation via Shuttleworth's equation and the Lippmann equation. Surface Science 601, 3042–3051.

Loh, K. J., Chang, D., 2011. Zinc oxide nanoparticle-polymeric thin films for dynamic strain sensing. Journal of Materials Science, 46, 228–237.

Okamoto, H., 1998. Cu-Mn (copper-manganese). Journal of Phase Equilibria, 19, 180.

Parida, S., Kramer, D., Volkert, C. A., Rösner, H., Erlebacher, J., Weissmüller, J., 2006. Volume change during the formation of nanoporous gold by dealloying. Physical Review Letters 97, 035504.

Pourbaix, M., 1966. Atlas of Electrochemical Equilibria in Aqueous Solutions. Pergamon Press, Oxford, U. K.

Pugh, D. V., Dursun, A., Corcoran, S. G., 2003. Formation of nanoporous platinum by selective dissolution of Cu from $Cu_{0.75}Pt_{0.25}$. Journal of Materials Research 18, 216–221.

Raney, M., 1927. Method of producing finely-divided nickel. US Patent 1628190.

Robertson, S. D., Freel, J., Anderson, R. B., 1972. The nature of Raney nickel VI. Transmission and scanning electron microsopy studies. Journal of Catalysis, 24, 130–145.

Schmickler, W., Leiva, E., 1998. A note on the surface stress and tension of solid metal electrodes. Journal of Electroanalytical Chemistry, 453, 61–67.

Sieradzki, K., Dimitrov, N., Movrin, D., McCall, C., Vasiljevic, N., Erlebacher, J., 2002. The dealloying critical potential. Journal of the Electrochemical Society, 149, B370–B377.

Smith, A. J., Munroe, P. R., Tran, T., Wainwright, M. S., 2001. FIB preparation of a sensitive porous catalyst for TEM elemental mapping at high magnifications. Journal of Materials Science 36, 3519–3524.

Weigend, F., Evers, F., Weissmüller, J., 2006. Structural relaxation in charged metal surfaces and cluster ions. Small 2, 1497–1503.

Weissmüller, J., Viswanath, R. N., Kramer, D., Zimmer, P., Wurschum, R., Gleiter, H., 2003. Charge-induced reversible strain in a metal. Science 300, 312–315.